Machine Learning-Enabled Uncertainty Quantification for Thermo-Catalytic Reactors: A Study on Fugitive Methane Oxidation in Monolith Reactors

Israfil Soyler[a,*], Cihat Emre Üstün[a], Amin Paykani[a], Xi Jiang[a], Nader Karimi[b]

[a]*School of Engineering and Materials Science, Queen Mary University of London, London, E1 4NS, United Kingdom*

[b]*School of Engineering, University of Southampton, Southampton, SO16 7QF, United Kingdom*

Abstract

Ultra-lean methane oxidation via catalytic combustion is critical for mitigating greenhouse gas emissions from fugitive methane sources. However, the catalytic oxidation process exhibits significant uncertainties that hinder its widespread implementation. To address this challenge, the present study develops a robust machine learning-based framework for quantifying combustion uncertainties, enabling more effective emission control strategies. The work presents a novel hybrid methodology integrating polynomial chaos expansion (PCE) with artificial neural networks (ANN), achieving real-time prediction of methane conversion rates and their uncertainties in monolith reactors. The machine learning model reduces computational time from hours to seconds while achieving excellent agreement with detailed 1D plug-flow reactor simulations. The investigation reveals that variations in methane concentration (0.2–1.3%, ±10%), inlet temperature (800–1000 K, ±2%), and inlet velocity (0.8–1.2 m/s, ±5%) significantly influence conversion uncertainty, with inlet temperature identified as the dominant parameter ($C_V \approx 75\%$). Stability improves at elevated temperatures (>950 K) and lower flow velocities ($C_V \approx 10\%$) compared to higher velocities (C_V = 17–22%). Additionally, catalyst deactivation, represented by reduced coating length, decreases methane conversion rates and increases uncertainty, with longer coatings providing greater stability at higher inlet temperatures. This work advances the fundamental understanding of uncertainty propagation in ultra-lean catalytic methane combustion and establishes a generalisable, computationally efficient PCE-ANN framework applicable to catalytic combustion of diverse fuels.

Keywords:

Fugitive methane; Ultra-lean catalytic combustion; Uncertainty quantification; Polynomial-chaos expansion (PCE); Machine learning (ANN); Monolith reactors.

*Corresponding author. Email: i.soyler@qmul.ac.uk

Latin Symbols

A	Arrhenius constant	OP	Orthogonal polynomials
ANNs	Artificial Neural Networks	P	Total order
C_k	PCE coefficients	PCE	Polynomial chaos expansion
CMC	Catalytic methane combustion	Pd	Palladium
CPU	Central processing unit	PDF	Probability Density Function
CSTR	Continuous stirred-tank reactor	PFR	Plug-flow reactor
d	Dimension	Pt	Platinum
E_a	Activation energy for the reaction	R	Universal gas constant
GHG	Greenhouse gas	R^2	Coefficient of determination
GPR	Gaussian Process Regression	R_c	Reactor catalyst coated length
GWP	Global warming potential	ReLU	Rectified Linear Unit
HPC	High performance computing	S_i	Main sensitivity of a fuel composition
IDT	Ignition delay time	S_L	Laminar flame speed
LU	Legendre-Uniform distribution	SFR	Stagnation-flow reactor
MAE	Mean Absolute Error	T_{in}	Inlet temperature
MC	Monte Carlo	UQ	Uncertainty quantification
ML	Machine learning	UQTk	Uncertainty Quantification Toolkit
NISP	Non-intrusive spectral projection	VAM	Ventilation air methane
NNs	Neural Networks	$Var[\beta]$	Total variance of methane conversion
n	Temperature exponent	V_{in}	Inlet velocity
N_{ord}	Parameter used for quadrature point generation		

Greek Symbols

β_{CH_4}	Uncertainty associated with catalytic methane conversion rate	μ_i	Rate coefficient dependences on the surface coverage
γ_θ	Relative uncertainty of input parameters	ξ	Quadrature points (germs)
Γ	Catalyst surface site density	π	Probability density function (PDF)
ε_i	Rate coefficient dependences on the surface coverage	σ	Standard deviation
θ	Randomly sampled input parameters	ϕ	Equivalence ratio
Ψ_k	Multidimensional orthogonal polynomials		

1. Introduction

Climate change, driven largely by greenhouse gas (GHG) emissions from human activities, is one of the most critical global challenges. Methane, CH_4, with a global warming potential 28-36 times higher than CO_2 over a 100-year period, has emerged as the second most significant anthropogenic GHG, contributing roughly 30% to global temperature rise [1, 2]. The energy sector is a major source of CH_4 emissions, with significant contributions from oil production (≈50

Mt), natural gas systems (≈30 Mt), and coal mining (≈40 Mt) annually [3]. In coal mining, ventilation air methane (VAM) which maintains CH_4 concentrations below 5 vol% for safety, accounts for over 70% of mine CH_4 emissions, despite its low concentration (≤1.5 vol%, typically <0.5 vol%) [4]. Mitigating these ultra-lean CH_4 emissions remains challenging due to operational issues such as large air volumes, fluctuating concentrations, dust, and humidity [5]. Conventional combustion requires CH_4 concentrations within flammability limits (5-17 vol%) and risks producing NO_x emissions at high temperatures [6]. Catalytic methane combustion (CMC) offers a superior alternative by enabling CH_4 oxidation at concentrations well below the flammability limit and at significantly lower temperatures (as low as 400 °C), substantially reducing both GHG impact and NO_x formation [7]. The oxidation process of CMC converts CH_4 to CO_2, a far less potent GHG, reducing the climate impact substantially. Additionally, capturing CH_4 from VAM exhaust is more challenging than absorbing CO_2 [7]. Thus, converting fugitive CH_4 to low-GWP CO_2 in the energy sector supports climate change mitigation and improves air quality.

Noble metal catalysts, particularly platinum (Pt) and palladium (Pd) on Al_2O_3 supports, are widely used for CMC due to their high activity and low-temperature CH_4 conversion rates [7]. While Pd-based catalysts exhibit higher activity, Pt catalysts are preferred for ultra-lean CH_4 combustion due to better resistance to poisoning and lower costs [8, 9]. Su and Yu [10] demonstrated this by developing a 25 kWe prototype using Pd/Al_2O_3 for lean-CH_4 combustion from VAM systems. The prototype successfully operated with 0.8% CH_4, generating 19-21 kWe without requiring cooling, air dilution, or nozzle injection. Burch et al. [11] compared Pt/Al_2O_3 and Pd/Al_2O_3 under various conditions, finding Pt superior in CH_4-rich environments and Pd more effective in O_2-rich (diluted) conditions. In addition to supported noble metals, recent reviews of Co_3O_4-based nanostructured catalysts, including noble metal doping strategies, have demonstrated the potential for enhanced catalytic performance and stability in lean methane combustion applications [12]. Furthermore, recent experimental studies on hierarchical monolith catalysts with self-supporting structures have demonstrated enhanced performance for lean methane catalytic oxidation [13].

Catalytic combustion in microreactors has gained attention due to their compact sub-millimetre-scale designs, offering advantages such as high surface-to-volume ratios, enhanced heat and mass transfer, and shorter diffusion times [9]. Honeycomb monolith reactors further improve performance with lower pressure drops, minimised external diffusion limitations, and prevention of

hotspots due to their structured channels (round, square, or finned) [9]. These channels can be coated with thin, uniform catalyst layers, increasing fuel-catalyst contact area and enabling efficient use of noble metals. He et al. [14] experimentally investigated Pt/γ-Al_2O_3 catalysts in various microreactor channel types for CH_4 combustion. They tested Pt loadings (1.5-5.0 wt%), CH_4 flow rates (150-500 mL/min), O_2:CH_4 ratios (0.5-6.0), and temperatures (300-500 °C), finding that CH_4 conversion increases with Pt loading but decreases with higher flow rates, especially at higher loadings. The optimal O_2:CH_4 ratio was 1.5 (vs. the stoichiometric 2.0), balancing O_2 and CH_4 on the catalyst surface. The double serpentine channel design achieved the highest CH_4 conversion due to its larger coating area, longer residence time, and improved gas mixing. Hunt et al. [15] studied ultra-lean CH_4 combustion in a wavy channel microreactor with Pt catalyst, showing that strategic catalyst placement (using only 25% of the coating) achieved 60% of the CO_2 production of fully coated channels. The wavy design increased CO_2 production rates, per unit surface area of the catalyst, by up to 400% compared to straight channels, highlighting the importance of channel configuration.

Dupont et al. [16] studied catalytic honeycomb monolith reactors with Pd and Pt catalysts for CH_4 combustion, highlighting their critical role in ignition and steady-state operation for complete CH_4 conversion to CO_2. They found that monolith length could be reduced by 70% (from 50.8 mm) without performance loss, as the reaction zone is confined to the first 10-15 mm of the channels, offering significant cost savings in noble metal usage. Higher flow rates, however, pushed the reaction zone deeper into the monolith and reduced combustion stability [16]. Kumaresh et al. [17] numerically studied lean CH_4 combustion in Pt-coated honeycomb monoliths, showing complete CH_4 conversion within 42 mm at 400 °C, 3% fuel/air ratio, and 20 m/s inlet velocity. Higher inlet temperatures and fuel/air ratios, combined with lower velocities, shifted the reaction zone upstream, reducing the required reactor length. Deutschmann et al. [18] numerically investigated CH_4 combustion on Pt foil using a detailed surface reaction mechanism, successfully predicting complex phenomena like ignition, extinction, and hysteresis [18].

VAM systems face significant variability challenges due to ultra-lean CH_4 concentrations (0.1-1.5%) and large ventilation air flows (100-300 m^3/s) [19]. These variations, caused by mining activities and underground pressure changes, affect gas quality, flow rate, and purity [4, 19]. Rahimi et al. [20] emphasised designing ventilation systems to account for gas emission uncertainties, ensuring safety against fires, explosions, and financial losses from coal seam gas fluctuations.

Combustion systems for VAM must handle these uncertainties, as sudden flow reductions disrupt combustion stability, while rapid CH_4 concentration increases risk equipment damage and higher NO_x emissions [9]. Additionally, low-concentration CH_4 often contains contaminants like dust, NO_x, H_2O, H_2S, and SO_2, which can poison and deactivate catalysts [9]. Catalyst deactivation in monolithic reactors remains a challenge due to uncontrolled emissions and incomplete combustion [21]. Temperature is critical, affecting reaction kinetics, catalyst activity, and stability. While catalytic combustion occurs at lower temperatures [7], precise temperature control is essential to avoid thermal stress, mechanical degradation, and accelerated deactivation [21, 22]. Uncontrolled temperature variations, especially when using waste heat, further complicate system performance [23]. These operational challenges underscore the need for systematic approaches to quantify and manage uncertainty in catalytic fugitive methane combustion.

Although previous studies discussed the presence of uncertainty in VAM systems, there remains a significant gap in the literature regarding systematic uncertainty quantification (UQ) in catalytic ultra-lean CH_4 combustion applications. Both experimental and computational approaches inherently contain unavoidable uncertainties, while traditional numerical models employ fixed parameters [24]. These uncertainties can be effectively quantified and reduced through mathematical modelling techniques. Uncertainties generally fall into two categories: epistemic and aleatoric. Epistemic uncertainty stems from lack of knowledge or information about the system and can potentially be decreased through improved understanding and enhanced measurement technique. Conversely, aleatoric uncertainty arises from the probabilistic nature of random processes and is irreducible, even with complete system knowledge [25]. In this study, the computational framework primarily focuses on epistemic uncertainty through the analysis of parametric variations in inlet conditions (temperature, velocity, and concentration) and catalyst coating length. These variations represent uncertainties that could theoretically be reduced with improved measurement, control systems, and catalyst design. By quantifying how these epistemic uncertainties propagate through the catalytic system, the parameters that contribute most significantly to variability in methane conversion performance can be identified. Uncertainty quantification methods use mathematical modelling to measure and manage uncertainties in experimental and computational settings [24, 26, 27]. While Monte Carlo (MC) methods traditionally address epistemic uncertainties, they are computationally expensive for complex models requiring large sample sizes [28]. Surrogate models, such as Gaussian processes [29, 30] or Polynomial Chaos Expansion (PCE)

[31, 32], provide efficient alternatives to computationally expensive MC methods for UQ. For complex simulations, UQ-PCE is more cost-effective and efficient than UQ-MC; several studies have successfully applied PCE-based UQ methods to combustion problems [33–36].

While PCE significantly improves efficiency for UQ, it still remains demanding for complex catalytic systems requiring high-fidelity simulations with detailed chemistry and transport phenomena. Soyler et al. [36] demonstrated this computational burden by using PCE for UQ in $NH_3/H_2/N_2$/air combustion, completing over 21,000 simulations (6000 CPU hours) on an HPC cluster. In a follow-up study, they performed 70,000 simulations to analyse uncertainties in partially cracked NH_3/syngas combustion [37]. Similarly, Zhang and Jiang [31, 38, 39] demonstrated the need for extensive simulations in PCE-based UQ for combustion research. This computational burden presents a significant obstacle to the practical implementation of UQ for real-world catalytic applications, particularly for real-time monitoring and control systems necessitating more efficient approaches. The novel integration of machine learning (ML) with UQ techniques offers a promising solution to overcome this limitation by drastically reducing computational costs while maintaining accuracy [40], and enabling robust analysis of uncertainty propagation in catalytic methane combustion systems. ML techniques efficiently capture complex relationships between uncertain parameters and system outputs, enabling analysis of non-linearities and interactions without extensive model evaluations. Recent research has explored various ML algorithms for combustion properties, including laminar flame speed (S_L) [41, 42], ignition delay time (IDT) [43], and reforming processes [44]. Amongst these approaches, artificial neural networks (ANNs) have proven their effectiveness in combustion applications and their ability to model highly non-linear relationships between multidimensional input and output spaces [45], making them especially suited for catalytic conversion processes where multiple interacting parameters influence reaction outcomes. ML-based UQ frameworks enable robust design and optimisation of catalytic reactors under varying conditions, making them particularly valuable for catalytic VAM systems, where real-time prediction and optimisation under uncertainty are critical for practical implementation.

To the best of authors' knowledge, no prior studies have explored ML-based UQ for catalytic combustion systems, revealing a significant research gap. While ML and UQ have been applied to combustion modelling, their integration for directly predicting uncertainty metrics in catalytic systems remains unexplored. This study addresses this gap by developing a novel ML framework to predict uncertainty bounds, sensitivity indices, and probabilistic performance metrics for catalytic

CH_4 oxidation. The specific objectives of this work include several key components. First, an ML model (ANN) for predicting catalytic CH_4 conversion rates in monolith reactors is developed and validated. Second, the effects of varying CH_4 concentration, inlet temperature, and inlet flow velocity on uncertainty in CH_4 conversion are quantified by using a surrogate UQ method (PCE). Third, the influence of catalyst deactivation on conversion performance and uncertainty propagation is investigated. Fourth, dominant parameters driving uncertainty in ultra-lean catalytic CH_4 combustion are identified. Finally, the computational efficiency of the PCE-ANN framework compared to conventional approaches is demonstrated.

Once trained, the ML model delivers a remarkable computational advantage, reducing analysis time from hours to seconds while preserving high-fidelity uncertainty predictions. This hybrid PCE-ANN approach advances catalytic systems modelling in two crucial dimensions: theoretically, by elucidating the nonlinear propagation mechanisms of parametric uncertainties through complex surface reactions; and practically, by providing rapid assessment tools essential for robust fugitive CH_4 oxidation technology design. By quantitatively mapping how input uncertainties transform into performance variability, this framework establishes science-based safety margins, optimise operating conditions, and implement targeted control strategies that maximise conversion reliability while minimising catalyst deactivation. The resulting decision support capability addresses a critical gap in the development of resilient catalytic combustion systems for GHG mitigation applications.

2. Methodology

2.1. Uncertainty quantification method

In this work, PCE was employed to construct a surrogate model for UQ using the open-source Uncertainty Quantification Toolkit (UQTk) version 3.1.4 [46]. The mathematical formulation of the PCE surrogate model is briefly described below. The uncertainty in simulation parameters is expressed as:

$$\theta_{\text{sample}} = \theta_{\text{mean}} \pm \sigma_\theta \times \xi_d \tag{1}$$

where θ_{sample} represents a randomly sampled set of parameters for catalytic CH_4 oxidation, such as inlet temperature (T_{in}), inlet velocity (V_{in}), or equivalence ratio (ϕ). The mean values of these parameters are denoted by θ_{mean}, and their standard deviations by σ_θ. The random variable

germs, $\xi_d = (\xi_{T_{\text{in}}}, \xi_{V_{\text{in}}}, \xi_\phi)$, are generated using orthogonal polynomials based on the distribution type [47, 48]. These germs represent the standardised basis for constructing PCE, where each element corresponds to a specific uncertain input parameter (inlet temperature, inlet velocity, and equivalence ratio, respectively). The orthogonal polynomials are selected to match the probability distribution of each parameter (Hermite polynomials for normal distributions and Legendre polynomials for uniform distributions), ensuring optimal convergence of the expansion. For this study, a Legendre-Uniform (LU) distribution was assumed, with random variables uniformly distributed in the interval $[-1, 1]$. The standard deviation of each parameter is calculated as follows:

$$\sigma_\theta = \theta_{\text{mean}} \times \gamma_\theta \tag{2}$$

where γ_θ represents the relative uncertainty: 5% for inlet velocity ($\gamma_{V_{\text{in}}} = 0.05$), 10% for equivalence ratio ($\gamma_\phi = 0.10$), and 2% for inlet temperature ($\gamma_{T_{\text{in}}} = 0.02$).

The number of quadrature points (ξ_d) is calculated as $(N_{\text{ord}})^d$, where $N_{\text{ord}} = P + 1$ is the expansion order, and d is the number of uncertain parameters. With $P = 5$, this results in $(5 + 1)^3 = 216$ quadrature points. Higher-order expansions can lead to excessive quadrature points without improving UQ results [36]. The selection of $P = 5$ was based on the authors' previous implementation in similar combustion UQ studies [36, 37], where they demonstrated that orders higher than $P = 5$ did not provide significant improvement in accuracy while substantially increasing computational cost. For this catalytic system with 3 uncertain parameters, $P = 5$ is sufficient to capture the output variance while maintaining computational load with 216 evaluation points per case.

The multidimensional PCE for catalytic CH_4 conversion is expressed as:

$$\beta_{\text{CH}_4} = \sum_{k=0}^{P} C_k \Psi_k(\xi_d) \tag{3}$$

where β_{CH_4} represents CH_4 conversion with quantified uncertainty, C_k are the PCE coefficients (spectral mode strengths), and $\Psi_k(\xi_d)$ are Legendre-Uniform orthogonal polynomials up to order P. The PCE coefficients are determined using the non-intrusive spectral projection (NISP) method via Gauss-Legendre quadrature integration:

$$C_k = \frac{1}{\langle \Psi_k^2(\xi) \rangle} \int_{-1}^{1} \beta(\xi) \Psi_k(\xi) \pi(\xi)\, d\xi, \quad k = 0, \ldots, P \tag{4}$$

where $\pi(\xi)$ is the probability density function, and ξ represents the germ samples for each input parameter.

In addition to quantifying uncertainties in CH_4 conversion, a variance-based global sensitivity analysis [49] was conducted to evaluate the impact of input uncertainties on output uncertainty. This method assesses how individual parameter uncertainties contribute to the total uncertainty in CH_4 conversion. The first-order sensitivity indices (S_i) are calculated as:

$$S_i = \frac{\sum C_i^2 \langle \Psi_i^2 \rangle}{\mathrm{Var}[\beta]} \tag{5}$$

where (i) denotes a specific input parameter, and $\mathrm{Var}[\beta]$ represents the total variance of CH_4 conversion. The total variance is expressed as:

$$\mathrm{Var}[\beta] = \sum_{k>0} C_k^2 \langle \Psi_k^2 \rangle \tag{6}$$

2.2. Validation of Surface Reaction Mechanism

The surface reaction mechanism developed by Deutschmann et al. [50] was used, comprising 24 chemical reactions involving 11 surface species and 7 gas-phase species (Table 1). Pt catalyst was modelled with a surface site density (Γ) of 2.72×10^9 mol/cm^2, where Pt(s) represents uncovered surface sites available for adsorption.

The mechanism was validated using two models: a stagnation-flow reactor (SFR) and a plug-flow reactor (PFR). The SFR configuration, where gas flow impinges perpendicularly onto a catalytic surface, is ideal for studying gas-surface interactions and reaction kinetics. Its 1D nature simplifies analysis by focusing on the centreline, where variables depend only on the distance from the surface, making it suitable for validating detailed reaction mechanisms [18].

For catalytic CH_4 combustion simulations in a SFR, Cantera [51] was used to solve the surface chemistry reactions. The simulations were conducted under specified initial conditions to validate the surface reaction mechanism. A premixed gas mixture of 9.5% CH_4 in air was introduced with a uniform inlet velocity of 6 cm/s at 100 mm from the catalytic surface. The initial CH_4-air mixture and surface temperatures were set to 300 K and 1000 K, respectively, under atmospheric pressure.

The surface reaction mechanism was validated against the results of Deutschmann et al. [18] using an SFR configuration. Fig. 1 compares species mole fractions as a function of distance from the catalytic surface. The continuous lines represent the current numerical results, while the

Table 1: Surface reaction mechanism for CH_4 combustion over Pt catalyst from Deutschmann et al. [50].

	Reaction	A **(cm, mol, s)**	n	E_a **(kJ/mol)**	ε_i, μ_i**(kJ/mol)**
(1)	$H_2 + 2Pt(s) \rightarrow 2H(s)$	4.60×10^{-2}			$\mu_{Pt(s)} = -1^*$
(2)	$2H(s) \rightarrow H_2 + 2Pt(s)$	3.70×10^{21}	0.0	67.4	$\varepsilon_{H(s)} = 6$
(3)	$H + Pt(s) \rightarrow H(s)$	1.00^*			
(4)	$O_2 + 2Pt(s) \rightarrow 2O(s)$	1.80×10^{21}	-0.5	0.0	
(5)	$O_2 + 2Pt(s) \rightarrow 2O(s)$	$2.30\times10^{-2*}$			
(6)	$2O(s) \rightarrow 2Pt(s) + O_2$	3.70×10^{21}	0.0	213.2	$\varepsilon_{O(s)} = 60$
(7)	$O + Pt(s) \rightarrow O(s)$	1.00^*			
(8)	$H_2O + Pt(s) \rightarrow H_2O(s)$	0.75^*			
(9)	$H_2O(s) \rightarrow H_2O + Pt(s)$	1.00×10^{13}	0.0	40.3	
(10)	$OH + Pt(s) \rightarrow OH(s)$	1.00^*			
(11)	$OH(s) \rightarrow OH + Pt(s)$	1.00×10^{13}	0.0	192.8	
(12)	$O(s) + H(s) \rightarrow OH(s) + Pt(s)$	3.70×10^{21}	0.0	11.5	
(13)	$H(s) + OH(s) \rightarrow H_2O(s) + Pt(s)$	3.70×10^{21}	0.0	17.4	
(14)	$OH(s) + OH(s) \rightarrow H_2O(s) + O(s)$	3.70×10^{21}	0.0	48.2	
(15)	$CO + Pt(s) \rightarrow CO(s)$	$8.40\times10^{-1*}$			$\mu_{Pt(s)} = 1$
(16)	$CO(s) \rightarrow CO + Pt(s)$	1.00×10^{13}	0.0	125.5	
(17)	$CO_2(s) \rightarrow CO_2 + Pt(s)$	1.00×10^{13}	0.0	20.5	
(18)	$CO(s) + O(s) \rightarrow CO_2(s) + Pt(s)$	3.70×10^{21}	0.0	105.0	
(19)	$CH_4 + 2Pt(s) \rightarrow CH_3(s) + H(s)$	$1.00\times10^{-2*}$			$\mu_{Pt(s)} = 0.3$
(20)	$CH_3(s) + Pt(s) \rightarrow CH_2(s) + H(s)$	3.70×10^{21}	0.0	20.0	
(21)	$CH_2(s) + Pt(s) \rightarrow CH(s) + H(s)$	3.70×10^{21}	0.0	20.0	
(22)	$CH(s) + Pt(s) \rightarrow C(s) + H(s)$	3.70×10^{21}	0.0	20.0	
(23)	$C(s) + O(s) \rightarrow CO(s) + Pt(s)$	3.70×10^{21}	0.0	62.8	
(24)	$CO(s) + Pt(s) \rightarrow C(s) + O(s)$	1.00×10^{18}	0.0	184.0	

$k = AT^n e^{(-E_a/RT)}$, k is the rate constant for the reaction, A is the Arrhenius constant, n is the temperature exponent, E_a is the activation energy for the reaction, and R is the universal gas constant.
ε_i and μ_i are the rate coefficient dependences on the surface coverage.
* symbol represents the sticking coefficient.

marker points show data from Deutschmann et al. [18]. The simulation captures the key features of species evolution: O_2 and CH_4 are consumed near the surface, while CO_2 and H_2O are formed. A small amount of CO appears as an intermediate species, peaking near the surface before being oxidised to CO_2. The excellent agreement between the simulations and reference data validates the implementation of the surface reaction mechanism.

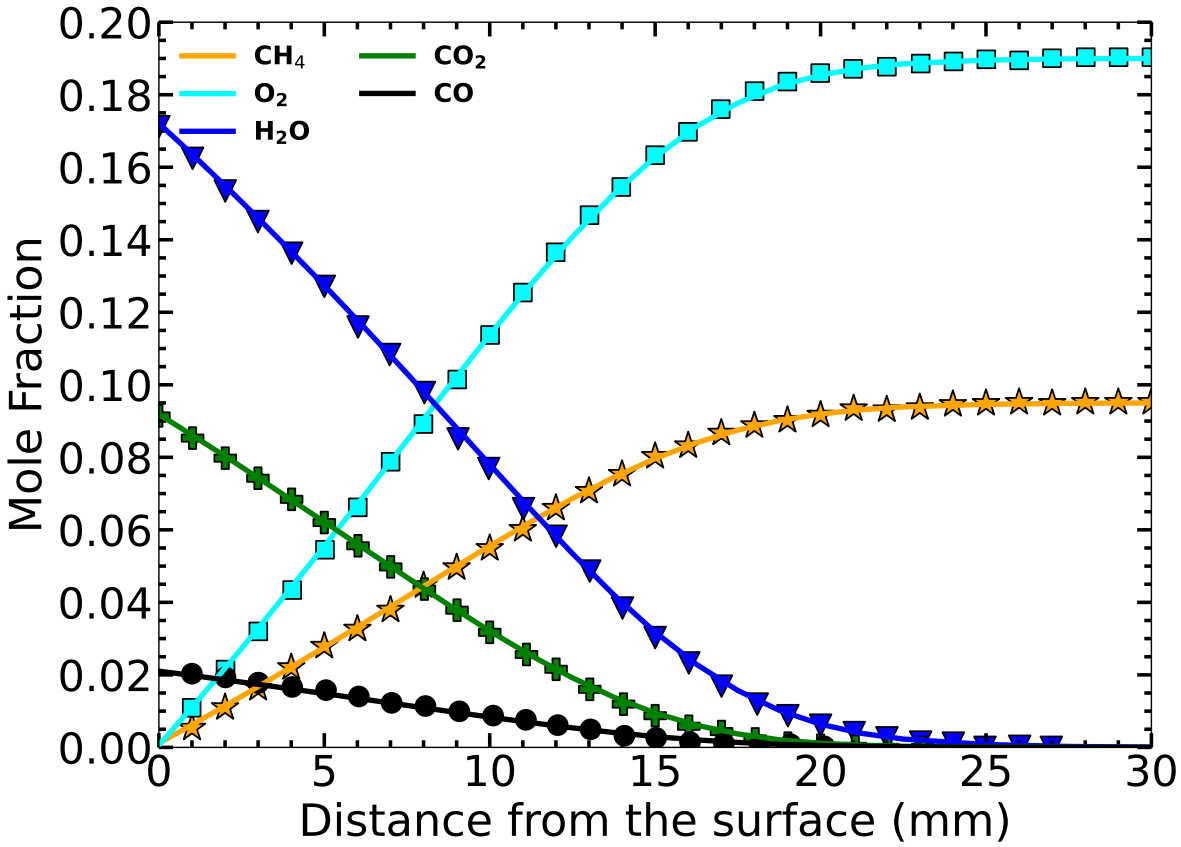

Figure 1: Validation of surface reaction mechanism using SFR simulations. Continuous lines represent numerical results from this study, while markers denote reference data from Deutschmann *et al.* [18].

The PFR represents a steady-state 1D flow system where species concentrations and temperature vary along the reactor length without diffusion. In this model, the reaction mixture flows uniformly at constant velocity, ensuring complete radial mixing and no backflow. The PFR is particularly suitable for catalytic systems, as surface reactions at the wall promote radial mixing. Its computational efficiency makes it an excellent tool for validating detailed kinetic mechanisms under steady-state conditions.

In this work, catalytic CH_4 combustion simulations were performed in a single-channel PFR with a length of 200 mm and a hydraulic diameter of 1.27 mm. The reactor simulated lean premixed CH_4-air combustion over a Pt catalyst at atmospheric pressure. Cantera was used to model the PFR as a chain of 201 continuous stirred-tank reactors (CSTRs). The governing equations for the 1D steady-state PFR model are detailed elsewhere [51]. The first CSTR was fed a lean CH_4/air mixture (fuel/air ratio 2.94%) at an inlet temperature of 645 °C and an inlet velocity of 16.7 m/s.

The surface reaction mechanism from Deutschmann et al. [50] was further validated against the results of Kumaresh and Kim [17] using a PFR configuration. Fig. 2 compares the current

results (continuous lines) with data from Kumaresh and Kim [17] (marker points). Initially, the Pt surface is predominantly covered by adsorbed oxygen O(s), with a coverage of approximately 0.9 at the reactor entrance.

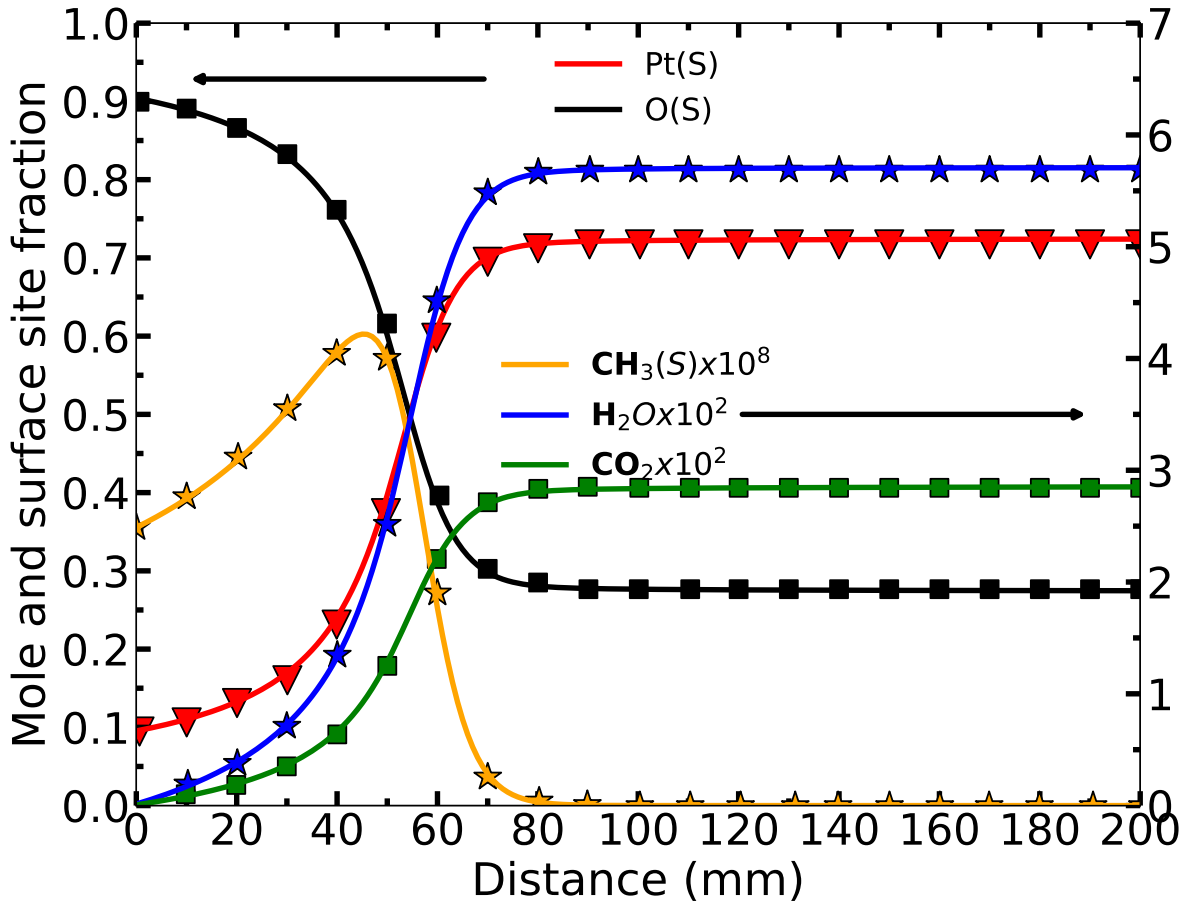

Figure 2: Validation of Deutschmann's surface mechanism with the results from Kumaresh and Kim by using PFR reactor. Continuous lines are from this study, marker points are from Kumaresh and Kim [17].

As reactions proceed, O(s) coverage decreases while free Pt(s) increases, stabilising at about 0.7 after 60 mm. The adsorbed methyl species CH_3(s) (scaled by 10^8 for clarity) peaks at 40-50 mm, indicating the region of most active CH_4 decomposition, before being consumed in subsequent reactions. The formation of CO_2 and H_2O (scaled by 10^2 for clarity) increases until reaching steady-state values after about 80 mm. The excellent agreement between our simulations and the reference data validates both the surface mechanism implementation and the PFR model assumptions in the specified conditions.

2.3. Machine learning (ML)

In this work, ML models were developed to predict how variations in input parameters affect ultra-lean catalytic CH_4 conversion rates, efficiently capturing complex reaction behaviours under different operational conditions. This section describes the data generation process, including associated uncertainties for 1D simulations using Cantera, followed by an introduction to the ANN methodology. Fig. 3 presents a detailed overview of the PCE-ANN framework employed in this study, illustrating the integration of UQTk, Cantera, ANN development, and potential applications.

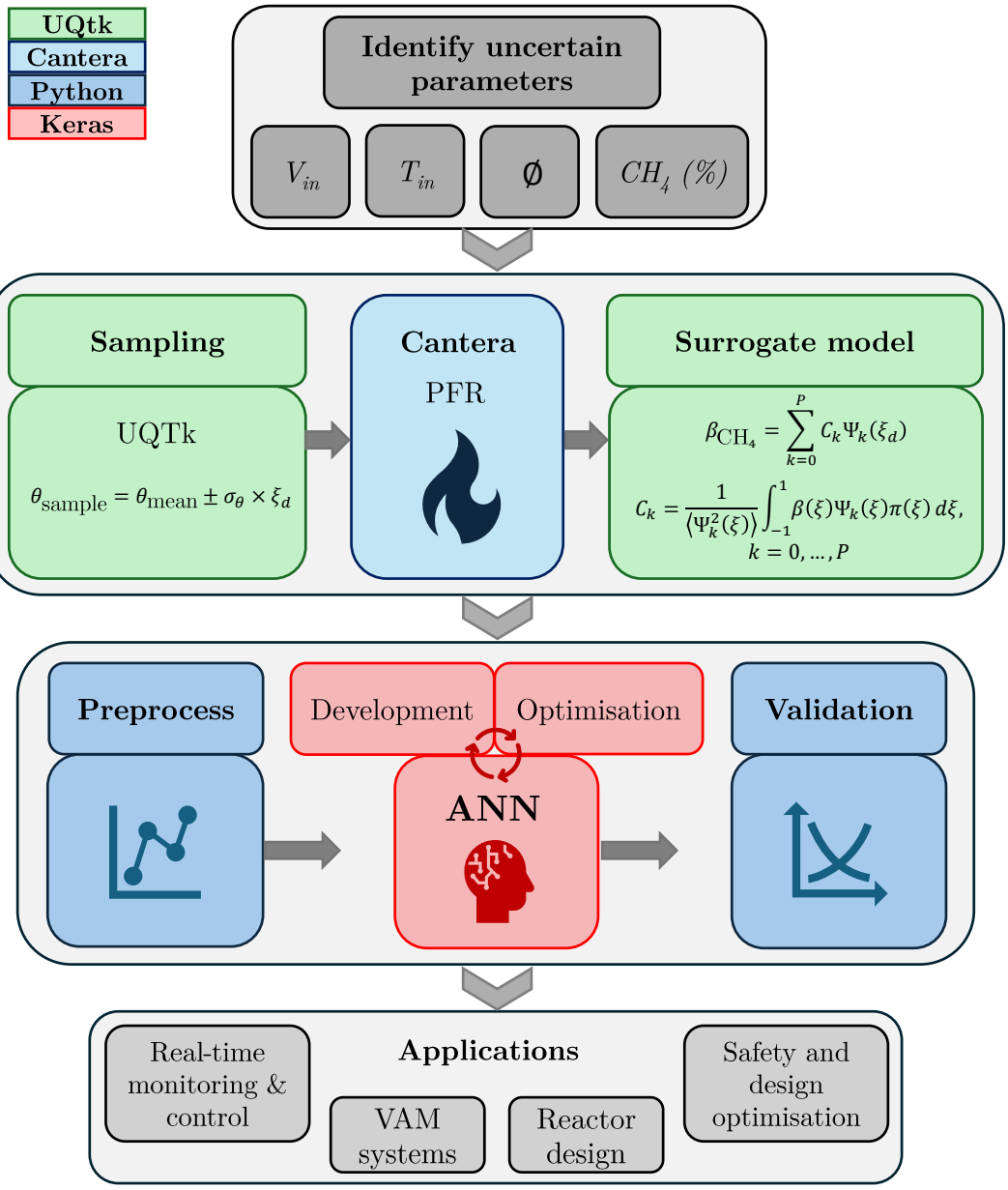

Figure 3: Overview of the PCE-ANN framework with potential applications.

2.3.1. Data Generation

Honeycomb monolith reactors are widely used for emission reduction due to their high surface area, low pressure drop, uniform flow distribution, thermal stability, durability, and versatility [52]. These reactors consist of numerous small-diameter channels coated with catalysts on their interior surfaces. In this work, a single channel is analysed, as each channel exhibits similar behaviour [50].

To train the ML models, operational input parameters with associated uncertainties were generated using UQTk software, and a comprehensive dataset was created through 1D simulations in Cantera [51]. The simulations focused on ultra-lean catalytic CH_4 combustion in a PFR, representing one channel of a honeycomb monolith reactor. A total of 180 cases were investigated, examining four key operational parameters (Table 2): CH_4 concentration in ventilation air (%), T_{in}, V_{in}, and catalyst length (R_c) in mm.

Ultra-lean CH_4 concentrations ranged from 0.2% to 1.3% in air, with ±10% uncertainty, reflecting varying emission scenarios and corresponding to ϕ of 0.017 to 0.138. Inlet temperatures varied from 800 K to 1000 K (±2% uncertainty), as temperature significantly impacts reaction kinetics and catalyst performance. Temperatures below 800 K were avoided due to insufficient O_2 desorption for CH_4 adsorption, while temperatures above 1200 K promote homogeneous CH_4 combustion without a catalyst [9]. Additionally, PtO_2, formed during catalytic oxidation, becomes unstable below 700 K [53], and temperatures above 900 K risk catalyst degradation and thermal NO_x formation. Inlet velocities ranged from 0.8 to 1.2 m/s (±5% uncertainty), capturing the effects of flow velocity on CH_4 conversion, residence time, and heat transfer.

Table 2: Data parameters with applied uncertainty used in ANN algorithm for 1D simulations.

CH_4 (%) ±10%			**T_{in} (K) ±5%**	**V_{in} (m/s) ±2%**	**Catalyst length(mm)**
CH_4 % in the air	**Equivalence Ratio (ϕ) Min/max**	**Mean**			
1.3	0.138/0.113	0.125	800-1000	0.8, 1.0, and 1.2	20, 30, and 50
0.9	0.095/0.078	0.086			
0.6	0.063/0.052	0.057			
0.2	0.021/0.017	0.019			

The UQ for each case required 216 individual simulations ($(5+1)^3 = 216$), as detailed in Section 2.1, due to the propagation of uncertainties through the system. This resulted in a total of 38,880 data points, sufficient for training reliable ANN models and accurately quantifying uncertainties.

2.3.2. Model Development and Optimisation

The relationship between ANN performance and architectural complexity is highly problem-dependent, necessitating a systematic evaluation of various configurations. Prior to ANN training, the input dataset underwent power transformation for normalisation and random shuffling to prevent sequence-based biases. Training employed a batch size of 128, a maximum of 3000 epochs, an initial learning rate of 5×10^{-3} with a decay rate of 1×10^{-4}, and the Adam optimiser with early stopping after 100 consecutive epochs without improvement in the loss function. The Rectified Linear Unit (ReLU) activation function was used across all hidden layers to mitigate gradient vanishing issues. The loss function, mean absolute error (MAE), is defined as:

$$\mathrm{MAE} = \frac{1}{m} \sum_{i=1}^{m} |\mathrm{CH_4\%} - \widehat{\mathrm{CH_4\%}}| \tag{7}$$

For ANN architecture optimisation, a design space of 2 to 10 layers and 4 to 40 neurons per layer was explored, encompassing 81 distinct ANN evaluations. This hyper-parameter optimisation study was completed in approximately 6 hours using an NVIDIA RTX 2000 Ada GPU, demonstrating the efficiency of modern computational resources.

The validation set loss term landscape (Fig. 4) revealed optimal configurations for predictive performance. The lowest MAE values were concentrated in regions with shallow networks (3-5 layers) and 10-15 neurons. The highest accuracy was achieved with a 4-layer, 32-neuron configuration (marked with a red star), chosen for the remainder of this study (Fig. 5). This architecture achieved an MAE of 0.062 with a minimal generalisation gap between train and validation losses. Networks with increased depth (5-10 layers) maintained stable performance across various neuron counts, suggesting width contributes more significantly to robustness than depth. The steepest error gradients occurred in the lower left corner, where the MAE values rapidly increased to 0.60 and above, indicating inadequate fitting. These findings highlight the importance of systematic hyper-parameter optimisation in ANN design.

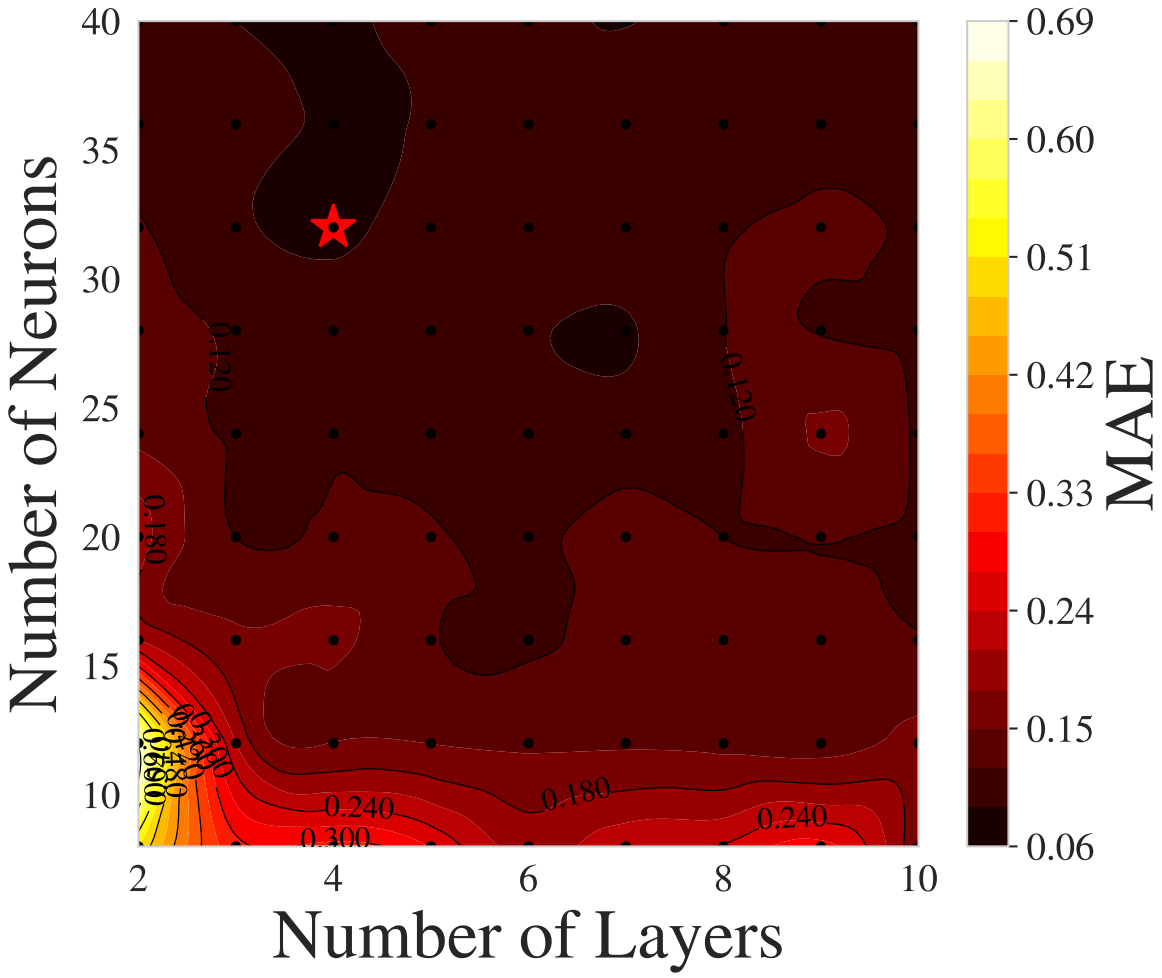

Figure 4: Accuracy map of ANN architectures in terms of neurons per hidden layer and hidden layers, represented by loss term on the validation set. The red star indicates the lowest MAE, while black circles denote individual ANN evaluations.

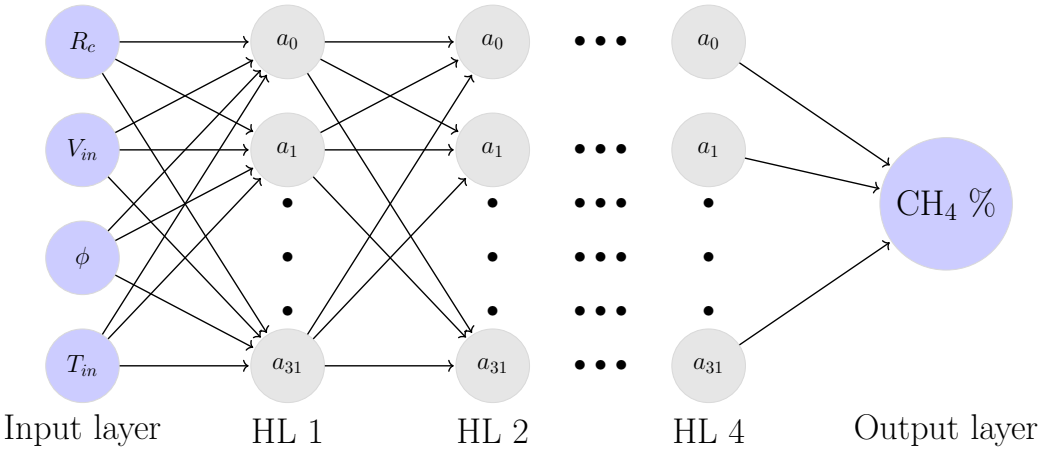

Figure 5: Schematic of the optimised neural network structure for the given dataset.

To ensure robust model validation, a 5-fold cross-validation strategy was implemented using

R^2 scoring (Eq. (8)) as the evaluation metric on the final model. The cross-validation results demonstrated negligible standard deviation and achieved $\overline{R^2} = 0.995 \pm 0.002$ with $\overline{MAE} = 0.068 \pm 0.013$.

$$R^2 = 1 - \frac{\sum_{i=1}^{m}(CH_4\%_i - \widehat{CH_4\%_i})^2}{\sum_{i=1}^{m}(CH_4\%_i - \overline{CH_4\%})^2} \tag{8}$$

The model's predictive accuracy was evaluated by comparing predicted values against ground truth data for the test set (Fig. 6). The comparison plot shows excellent agreement between predictions and actual values across the full range of CH_4 conversion rates (0-100%). Data points closely follow the ideal diagonal line, indicating strong predictive performance. The colour gradient, representing temperature (800-1100 K), demonstrates consistent accuracy across all temperature ranges, with no significant bias or degradation at extremes. The tight clustering of test set predictions along the diagonal confirms the model's ability to generalise to unseen data without over fitting, validating the chosen architecture and training parameters.

In terms of computational performance, a direct quantitative comparison is not rigorous due to differences in compute resources. Training of the final ML model took around 10 CPU hours on a 13th Gen Intel i7-13850HX CPU. Once trained, the ANN model achieves remarkably fast batch inference, processing the entire training dataset of 38,800 data points in 0.2 seconds on a single CPU, while data generation required approximately 2,500 CPU hours on a high-performance computing cluster.

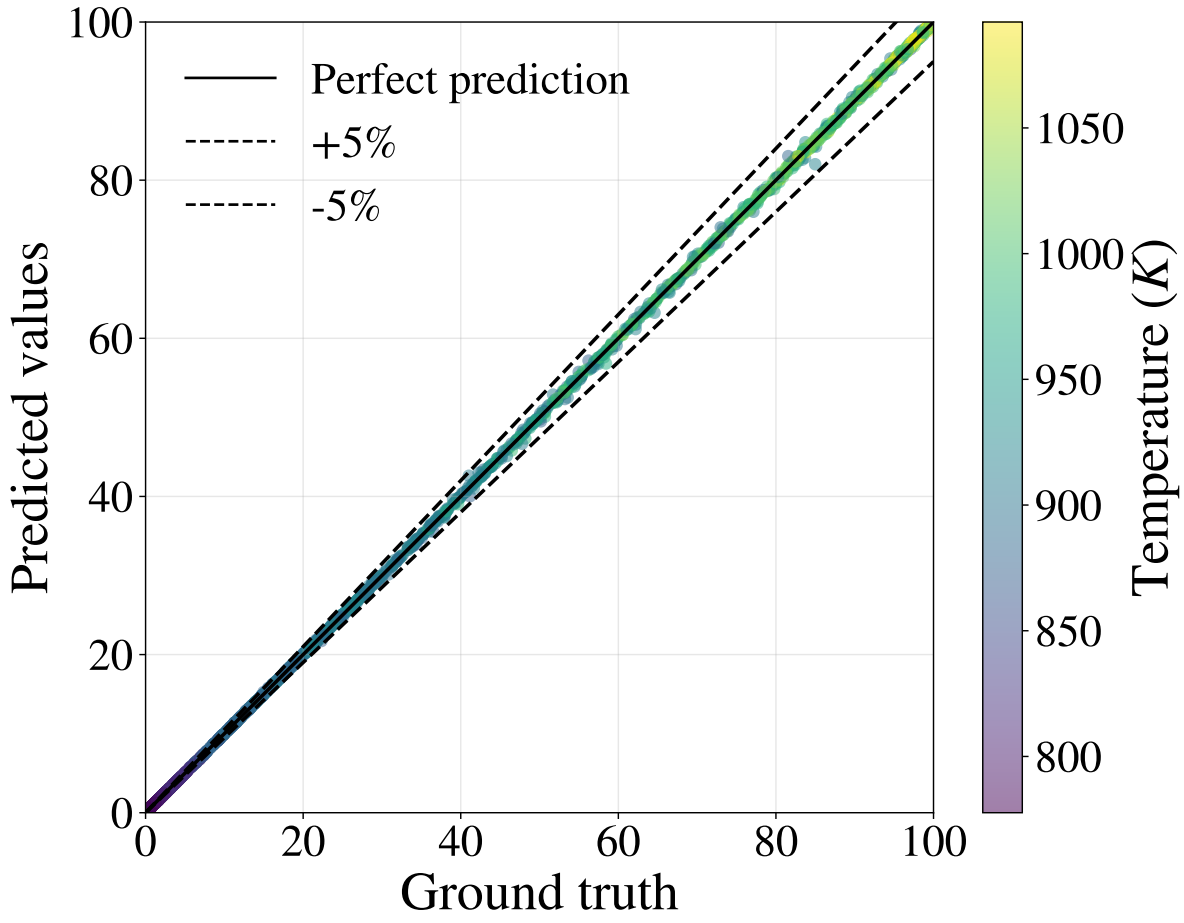

Figure 6: Ground truth versus predicted values for the test set using the optimal ANN architecture. The dashed lines represent ±5% of the ground truth values.

2.3.3. Model Validation

The ML model was validated against 1D Cantera simulations by comparing probability density functions (PDFs) of CH_4 conversion for different operating conditions. The Cantera simulations used a PFR model, which assumes perfect radial mixing and considers axial variations in species concentrations and temperature. This model is suitable for monolithic reactor channels due to their high length-to-diameter ratio and laminar flow conditions. In UQ studies, validating PDF results is critical, as it demonstrates the model's ability to predict the mean values and the complete distribution of outcomes and their likelihood. This is essential for understanding uncertainty propagation and assessing prediction reliability under varying conditions.

Fig. 7 compares PDFs for various inlet velocities (V_{in} = 0.8, 1.0, and 1.2 m/s) and temperatures (850 K to 950 K). The ML model shows excellent agreement with Cantera results across all conditions, accurately capturing both the magnitude and shape of the PDF distributions. This indicates that the ML model has successfully learned the underlying uncertainty propagation mechanisms in the system.

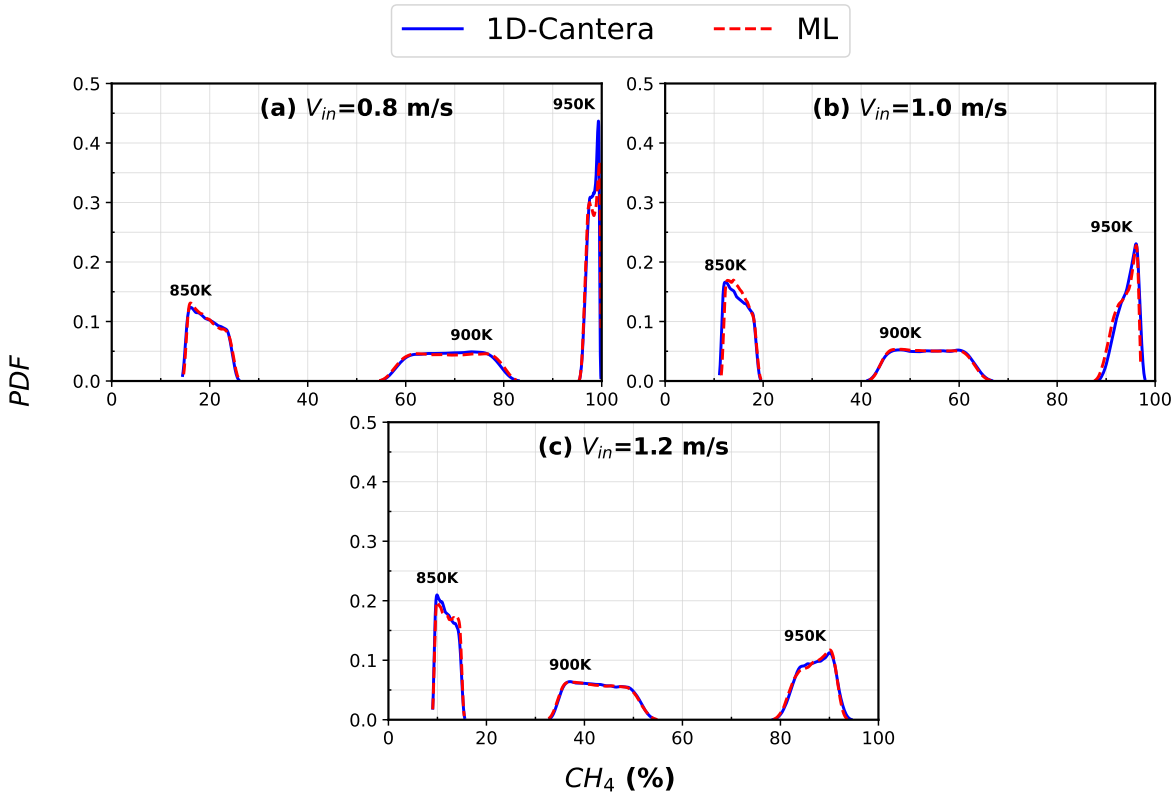

Figure 7: Validation of CH_4 conversion from Cantera and ML at different T_{in} and V_{in}: **(a)** 0.8 m/s, **(b)** 1.0 m/s, **(c)** 1.2 m/s.

3. Results and Discussion

3.1. Effects of CH_4 Concentration in Air

The effects of CH_4 concentration on the uncertainty in CH_4 conversion were analysed for various T_{in}, with a constant coated channel length of 50 mm and V_{in} of 0.8 m/s. Fig. 8 shows CH_4 conversion as a function of T_{in}, where continuous lines represent mean conversion values, and shaded areas indicate uncertainty bands. Both CH_4 concentration and T_{in} significantly influence the conversion rate and its uncertainty. As concentration increases from 0.6% to 1.3%, the coefficient of variance (C_V) peaks at approximately 75% at 850 K for 1.3% CH_4, indicating higher variability in conversion rates. However, uncertainty decreases significantly at elevated temperatures (>950 K), regardless of CH_4 concentration, demonstrating more stable operations at higher temperatures.

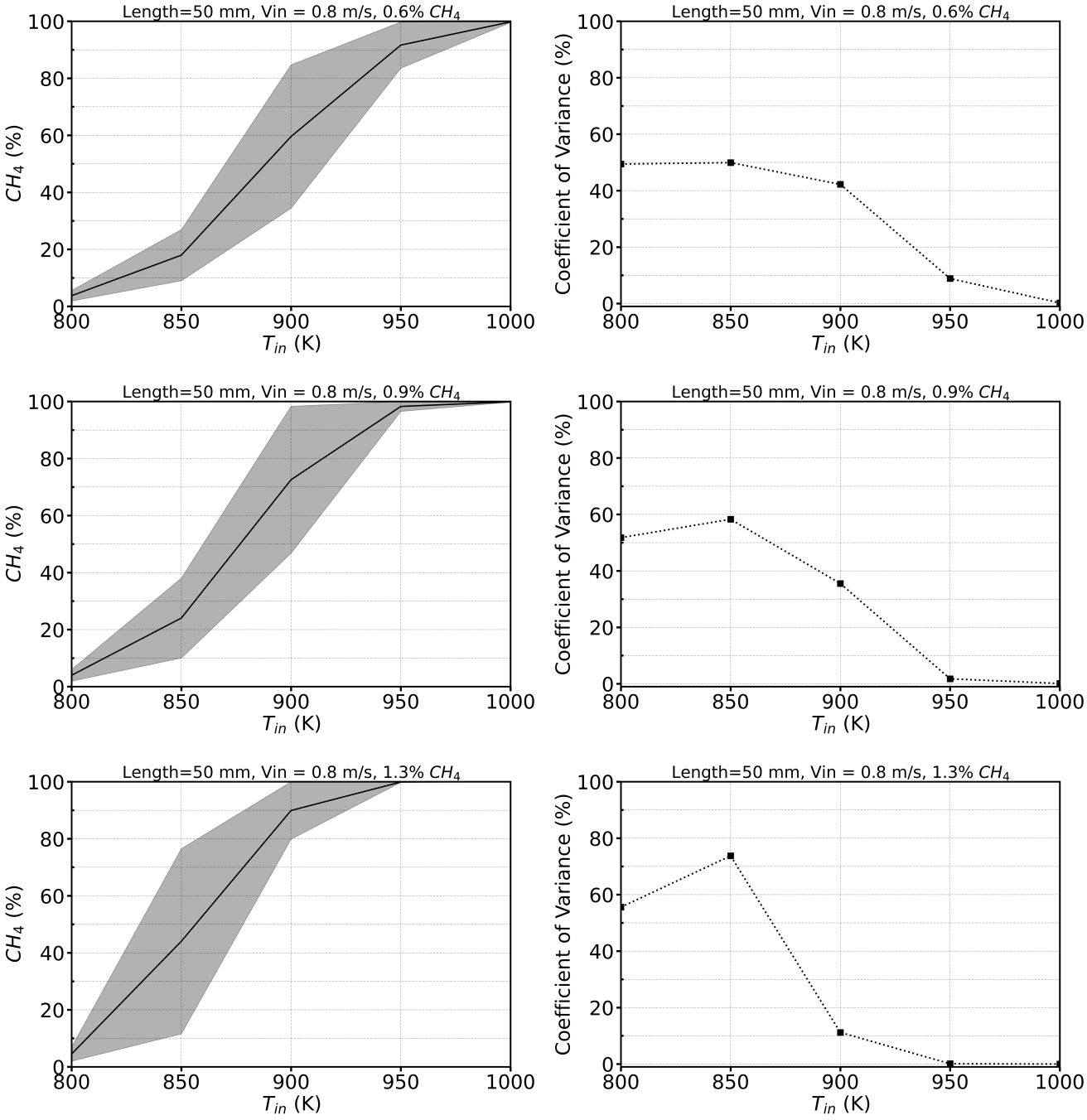

Figure 8: Effect of uncertainty on CH_4 conversion for different inlet temperatures. Continuous lines represent the mean conversion values, while shaded areas indicate the uncertainty bands due to the deviations in input parameters.

For further insight, Fig. 9 shows PDFs of CH_4 conversion rates at various temperatures and CH_4 concentrations. At lower T_{in} (850 K), PDFs for higher CH_4 concentrations exhibit wider distributions, consistent with the uncertainty bands in Fig. 8. As T_{in} increases, PDFs for higher CH_4 concentrations become narrower and sharply peaked in the high conversion region (80-100%), supporting the stability of CH_4 conversion at elevated temperatures.

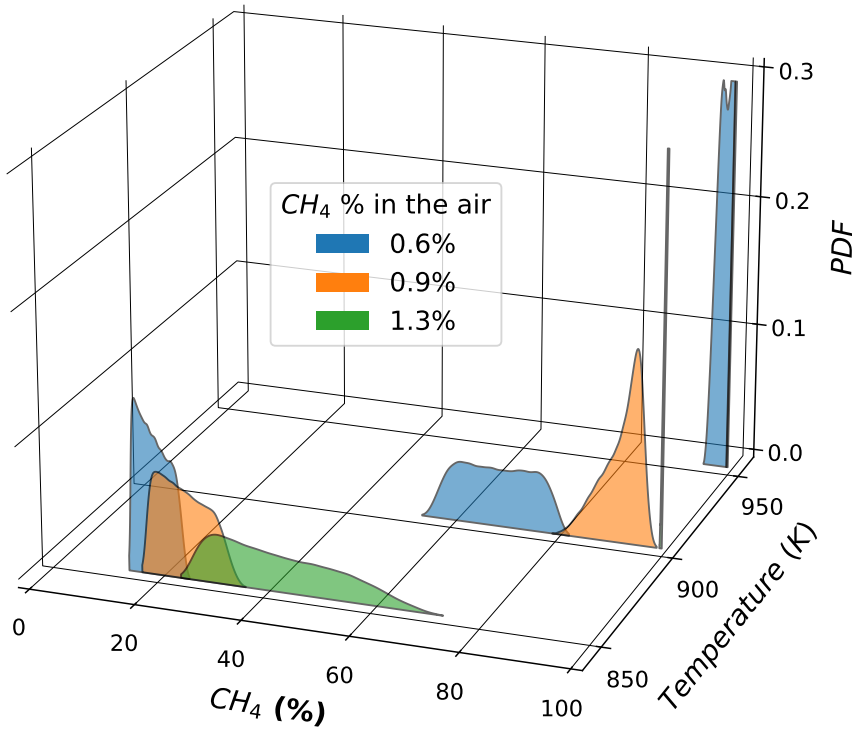

Figure 9: PDFs for different CH_4 concentrations in air at various temperatures.

3.2. Effects of Inlet Velocity (V_{in})

Inlet velocity, which controls ventilation air flow, is critical for safety and emission control in industrial settings. Higher ventilation rates ensure safer conditions by diluting CH_4 below explosive limits but reduce catalytic conversion efficiency by decreasing residence time. The effect of V_{in} on CH_4 conversion uncertainty was analysed for three velocities (0.8, 1.0, and 1.2 m/s) at a constant CH_4 concentration of 0.6% and a catalyst-coated channel length of 50 mm. Fig. 10 shows that CH_4 conversion rates are consistently higher at lower V_{in}, attributed to increased residence time. While C_V values are similar (around 50%) at 800 K, they diverge with increasing T_{in}. For

V_{in} = 0.8 m/s, C_V decreases rapidly to 10% at 950 K, whereas higher V_{in} (1.0 and 1.2 m/s) show slower decreases, reaching 17% and 22%, respectively. These results highlight the trade-off between safety and conversion efficiency, emphasising the need to optimise operating temperatures based on ventilation rates.

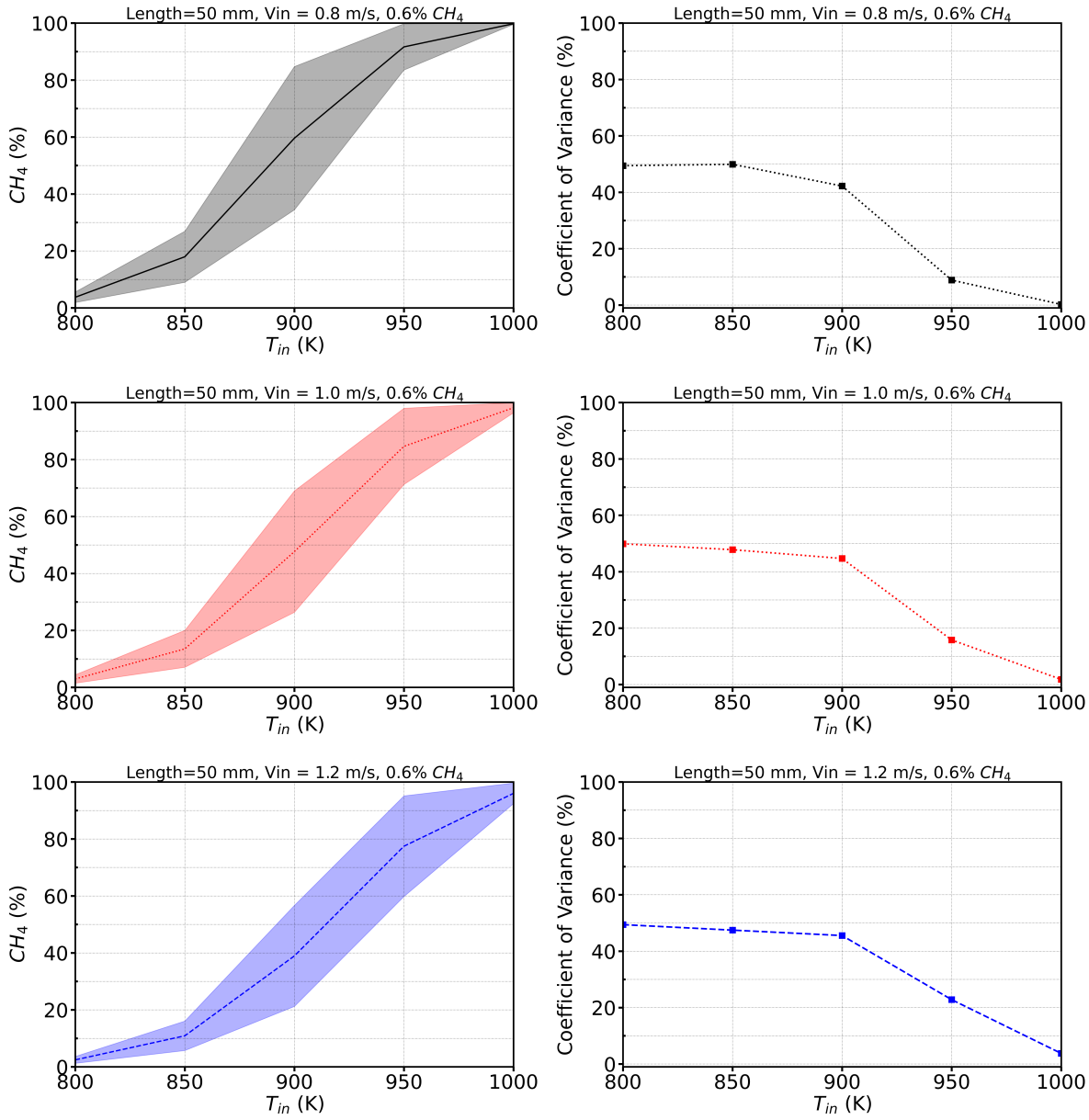

Figure 10: Comparison of uncertainty effects on CH_4 conversion for 0.6% CH_4 in air at different inlet velocities. Continuous lines represent the mean conversion values, while shaded areas indicate the uncertainty bands due to the deviations in input parameters.

For further analysis, Fig. 11 shows PDFs of CH_4 conversion at different V_{in} and T_{in} for a 50 mm catalyst-coated reactor with 0.6% CH_4 in air. At 950 K, CH_4 conversion exhibits reduced uncertainty with narrower PDFs at lower V_{in}. However, at 900 K, PDFs are wider and less

stable regardless of V_{in}, highlighting the importance of temperature control in achieving consistent conversion rates.

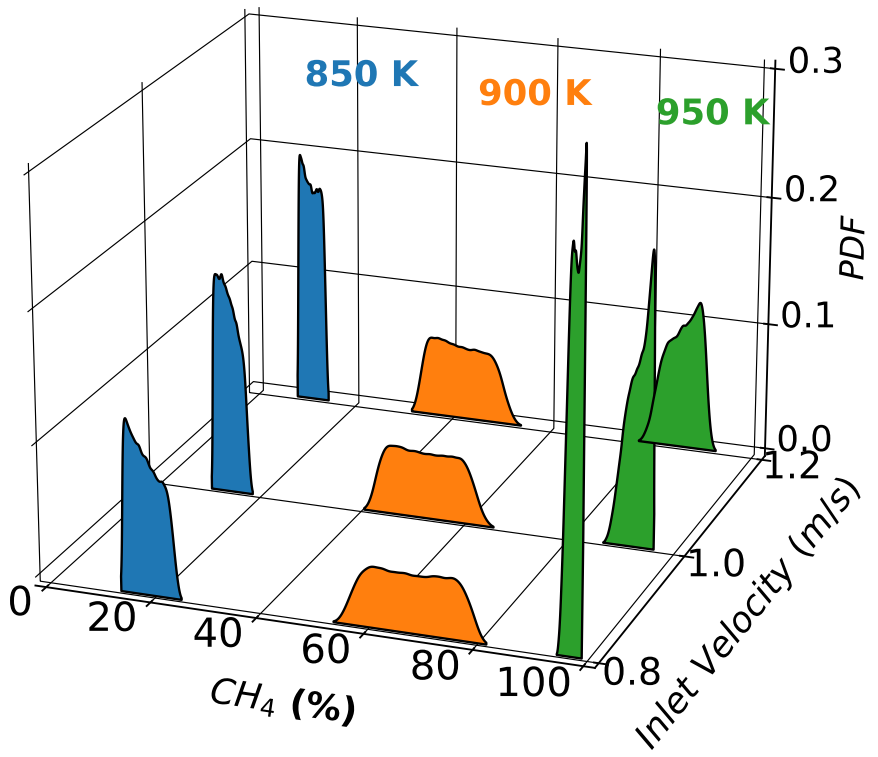

Figure 11: PDF comparison of CH_4 conversion for different T_{in} and V_{in} for a 50 mm catalyst-coated reactor with 0.6% CH_4 in air.

3.3. Effect of Inlet Temperature (T_{in})

Inlet temperature plays a crucial role in CH_4 conversion, as higher temperatures enhance catalyst activity, promoting more complete conversion. Fig. 12 shows the effects of T_{in} on CH_4 conversion rates and their associated uncertainties for different CH_4 concentrations. At lower T_{in} (850 K), CH_4 conversion rates are low due to limited catalytic activity, increasing gradually from 15% at 0.2% CH_4 to 45% at 1.3% CH_4. Uncertainty also increases with T_{in}, peaking at 75% for 1.3% CH_4, consistent with the discussion in **Section** 3.1. At higher T_{in} (>900 K), C_V decreases with CH_4 concentration, indicating more stable conversion. For T_{in} = 950 K, CH_4 conversion rates reach 60-100%, with complete conversion at 1.3% CH_4, demonstrating that elevated temperatures enhance both conversion rates and process stability.

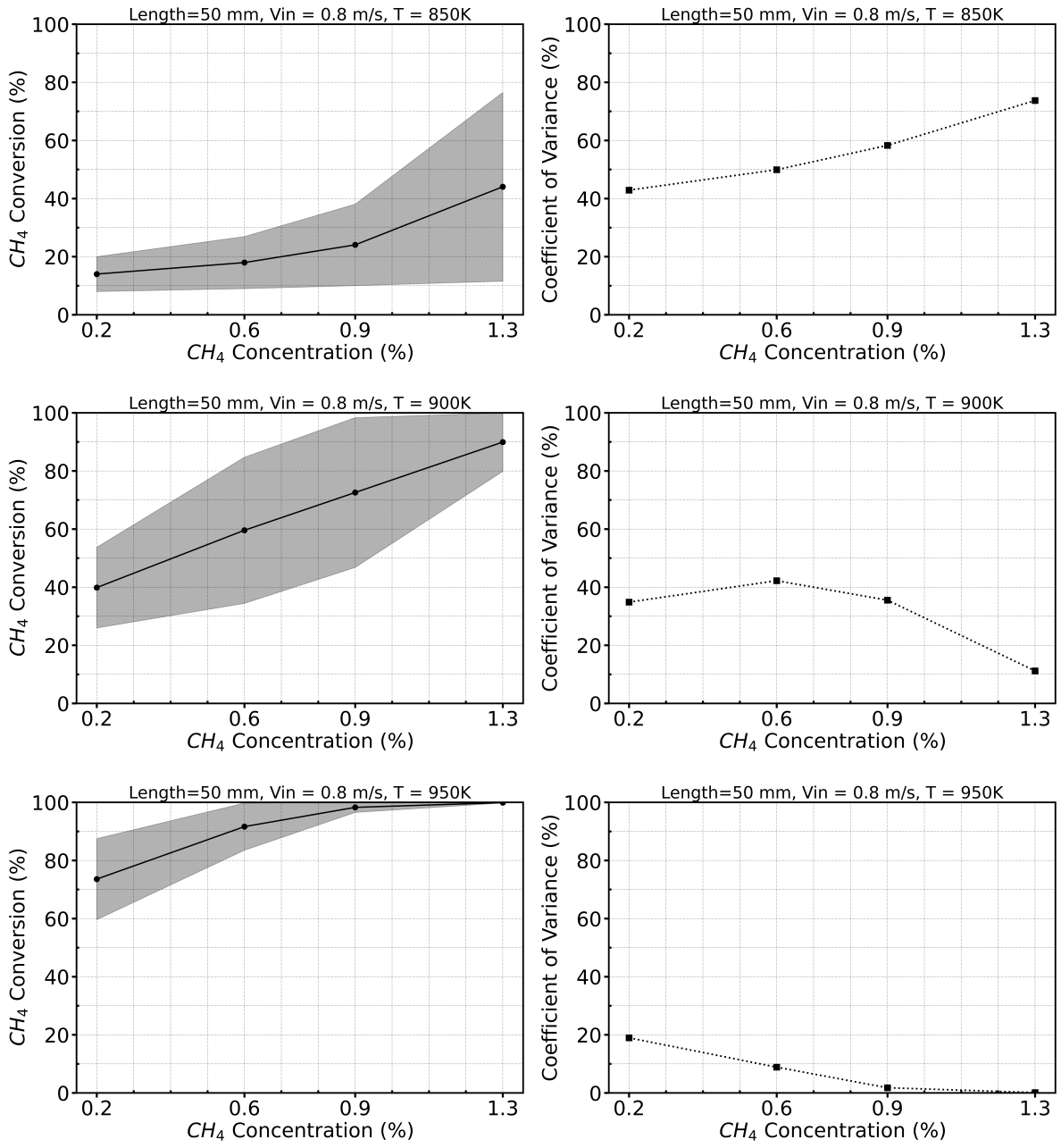

Figure 12: Effect of uncertainty on CH_4 conversion for different CH_4 concentrations in air at various temperatures. Continuous lines represent the mean conversion values, while shaded areas indicate the uncertainty bands due to the deviations in input parameters.

While V_{in} affects CH_4 conversion uncertainty by influencing residence time, T_{in} has a more fundamental impact. Fig. 13 shows the main sensitivity analysis for various T_{in} and CH_4 concentrations (0.2% to 1.3%) at different V_{in}. T_{in} is the primary contributor to uncertainty, especially at lower T_{in} and CH_4 concentrations. Its contribution decreases with increasing T_{in} and CH_4 concentration, while the impact of CH_4 concentration (ϕ) and V_{in} becomes more significant. At higher T_{in} (950 K) and CH_4 concentrations, the order of contribution to uncertainty is $T_{in} > \phi > V_{in}$, highlighting the importance of temperature control for stability at lower equivalence ratios and flow velocities.

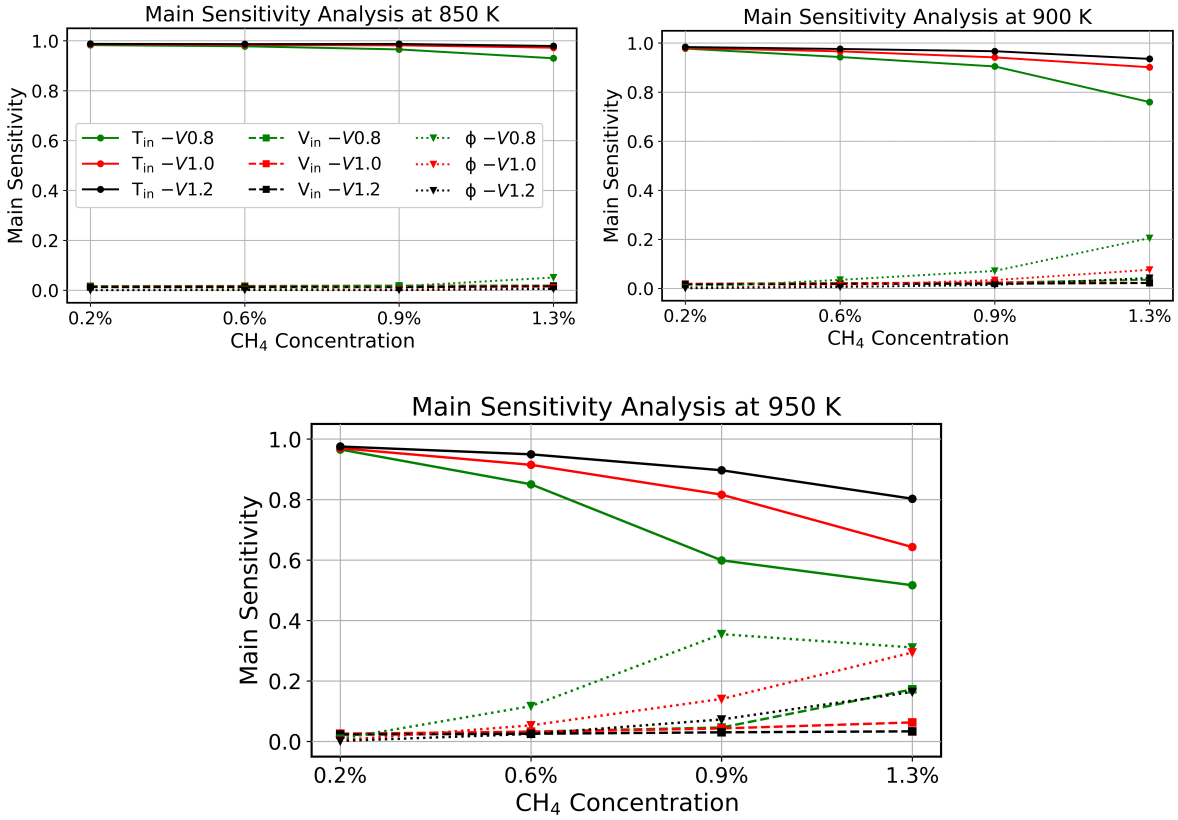

Figure 13: Main sensitivity analysis at various T_{in} and CH_4 concentrations for different inlet velocities.

3.4. Effects of Catalyst Coating Length

Catalyst deactivation is a significant challenge in real catalytic CH_4 conversion reactors, particularly in systems processing low-concentration CH_4 in air, which often contains contaminants such as dust, NO_x, H_2O, H_2S, and SO_2. These impurities can degrade catalyst performance or cause complete deactivation [9]. To understand the impact of deactivation, three catalyst coating lengths (50, 30, and 20 mm) were analysed, representing varying stages of catalyst availability.

These reduced coating lengths serve as a simplified representation of the effective active catalyst area remaining after partial deactivation. While this approach does not capture the full complexity of deactivation dynamics, it provides valuable insights into how reduced catalyst availability affects both conversion efficiency and process predictability. Fig. 14 shows that shorter coating lengths lead to lower CH_4 conversion rates and higher uncertainty. C_V values decrease with increasing T_{in}, but this decrease is less pronounced for shorter coating lengths, indicating that catalyst deactivation reduces both conversion efficiency and process predictability. Specifically, at T_{in} = 850 K, reducing coating length from 50 mm to 20 mm decreases mean CH_4 conversion from approximately 20% to 10%, while C_V decreases from 50% to 45%. The more dramatic effect is seen at higher temperatures (T_{in} = 950 K), conversion drops from nearly 100% to 60%, demonstrating that deactivation has greater absolute impact at conditions where the fresh catalyst would otherwise achieve complete conversion. Critically, the uncertainty (C_V) remains elevated even at high temperatures when catalyst is deactivated. For the 50 mm coating, C_V drops to 5% at 950 K, indicating very stable conversion performance. However, for the 20 mm coating, which represents around 60% deactivation, C_V remains at 35% even at 950 K. This persistent uncertainty under deactivated conditions has important implications: operators cannot compensate for deactivation simply by increasing temperature, as the system becomes inherently less predictable and more sensitive to input variations.

It should be noted that the representation of deactivation solely by reduction in coating length is a simplification of the complex deactivation phenomena occurring in real systems. In practice, catalyst deactivation can occur through multiple mechanisms, including poisoning by sulphur compounds, H_2O vapour, sintering at higher temperatures, and fouling by dust particles, which may alter not only the available surface area but also the intrinsic catalytic activity of remaining sites. The current simplified model assumes that the remaining catalyst maintains its original activity while the "deactivated" region has zero activity, which may not fully capture scenarios where poisoning or sintering reduce the intrinsic activity across the entire catalyst bed. Despite these limitations, this approach provides valuable first-order insights into how reduced catalyst availability affects conversion performance and uncertainty propagation, with the key finding that deactivation increases conversion uncertainty expected to be robust regardless of the specific deactivation mechanism.

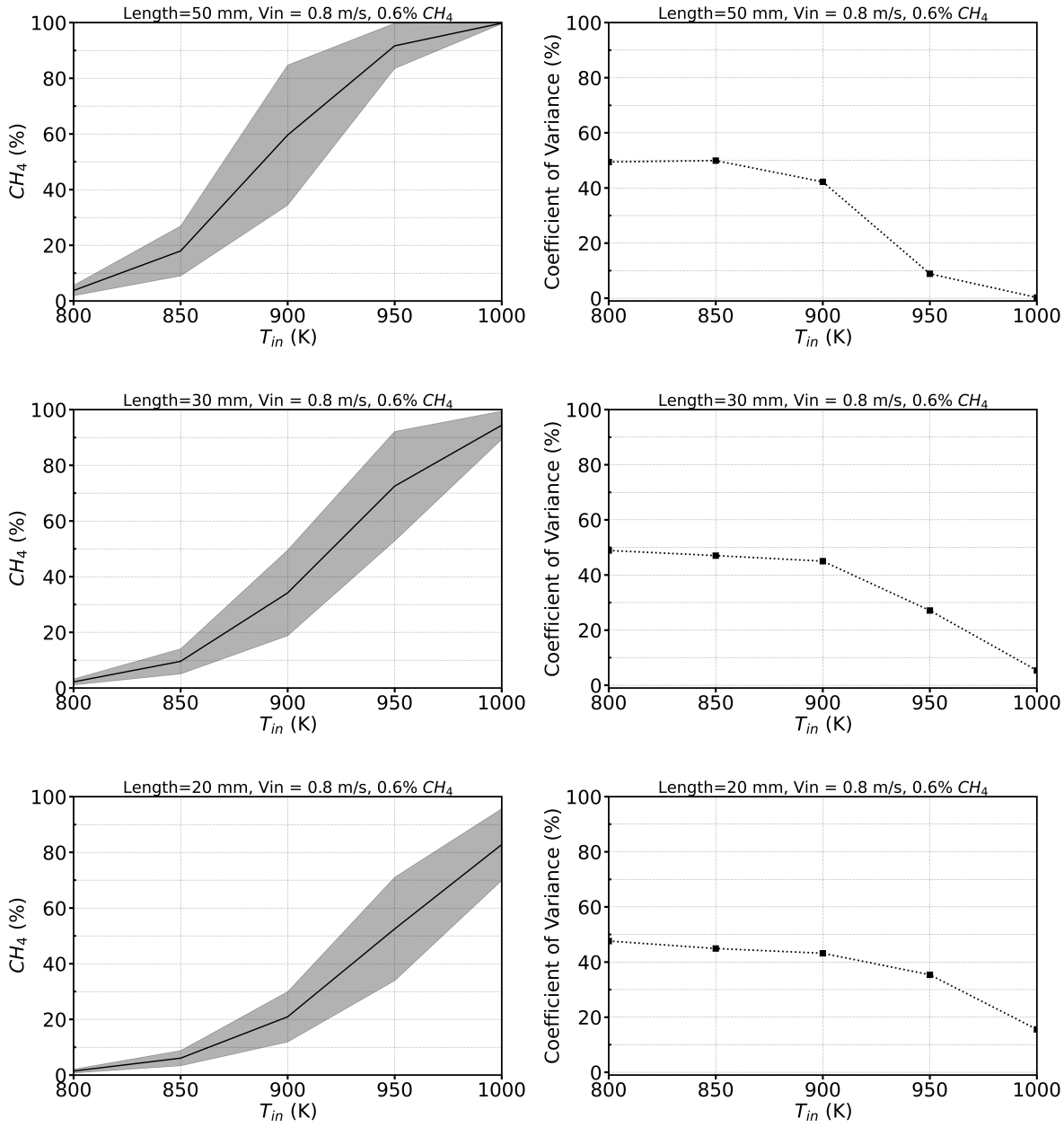

Figure 14: Effect of catalyst coating length in the monolith channel on CH_4 conversion rate and uncertainty. Continuous lines represent the mean conversion values, while shaded areas indicate the uncertainty bands due to the deviations in input parameters.

For further illustration, Fig. 15 shows PDFs of CH_4 conversion at 950 K for 0.6% CH_4 in air, comparing different V_{in} and catalyst coating lengths. Longer coating lengths result in higher conversion rates and more stable performance, evidenced by narrow, sharply peaked PDFs centred at high conversion values. For V_{in} = 0.8 m/s with 50 mm coating, the PDF shows a sharp peak at 95% conversion with minimal spread, indicating consistent, reliable performance. In contrast, the 20 mm coating produces a broader PDF centred at around 75% conversion, with significant

probability mass between 60-85%. This wider distribution indicates that under identical operating conditions, the partially deactivated catalyst produces highly variable outcomes, sometimes achieving acceptable conversion, other times falling well below target performance. This effect is more pronounced at higher V_{in} (1.2 m/s), where the reduced residence time exacerbates the impact of deactivation. The 20 mm coating at high velocity produces the broadest PDF, spanning 40-70% conversion, making performance prediction difficult and control strategy implementation challenging. These results highlight that catalyst deactivation not only reduces mean CH_4 conversion rates but also fundamentally alters the system's uncertainty characteristics, increasing operational risk and reducing process reliability. For $V_{in} = 0.8$ m/s, shorter coatings result in broader PDFs with lower peak heights, indicating less stable and lower conversion outcomes. This effect is more pronounced at higher V_{in}, aligning with the analysis in **Section** 3.2. These results highlight that catalyst deactivation not only reduces CH_4 conversion rates but also increases uncertainty, emphasising the need for regular monitoring and maintenance, especially at higher flow rates.

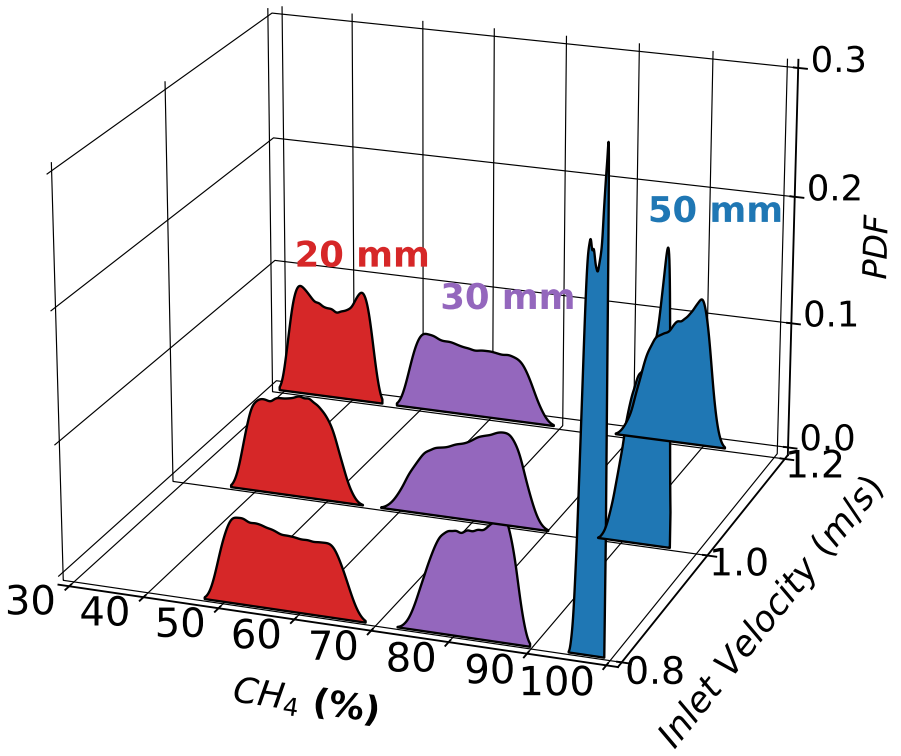

Figure 15: PDF comparison of CH_4 conversion at different V_{in} for various catalyst coating lengths at 950 K and 0.6% CH_4 concentration in air.

4. Conclusions

In this work, the effects of variability in ultra-lean fugitive methane combustion were investigated for various CH_4 concentrations ranging from 0.2% to 1.3% in air with ±10% uncertainty, corresponding to equivalence ratios (ϕ) between 0.017 and 0.138. Additionally, variations in inlet temperatures from 800 K to 1000 K (±2% uncertainty) and inlet velocities from 0.8 to 1.2 m/s (±5% uncertainty) were analysed for various catalyst lengths (20, 30, and 50 mm). The study employed the validated Deutschmann et al. [18] mechanism to simulate a PFR model for 1D catalytic CH_4 combustion over a Pt catalyst. For the first time, a data-driven PCE-based UQ method was applied to investigate the impact of small parameter variations on CH_4 conversion in a PFR, representing a single channel of a honeycomb reactor. Additionally, catalytic CH_4 conversion, along with associated uncertainty, was successfully modelled and predicted using an ML approach via an ANN.

Key findings from this study are as follows:

- The ANN model not only showed excellent agreement with 1D PFR simulations under various conditions but also demonstrated strong agreement with probability distributions arising from parameter uncertainties while reducing computational time from hours to mere seconds.
- Uncertainty in catalytic CH_4 conversion increases with fugitive CH_4 concentration in air, with a C_V reaching 75% for a 1.3% CH_4 concentration at $T_{in} = 850$ K.
- The uncertainty effect diminishes significantly as T_{in} increases, particularly for $T_{in} > 950$ K, where the catalytic process becomes more stable regardless of methane concentration.
- Catalytic CH_4 conversion is more stable at lower velocities, with C_V rapidly decreasing to about 10% at 950 K, whereas at higher velocities, C_V remains in the range of 17–22% under the same conditions.
- CH_4 conversion rate decreases while uncertainty increases as the catalyst-coated channel length decreases across all operating temperatures. This effect is more pronounced at higher flow velocities.
- Inlet temperature emerged as the dominant factor affecting uncertainty, irrespective of other parameters.

These findings underscore the crucial role of temperature control and regular catalyst maintenance, particularly when higher ventilation rates are required for safety. Overall, parameter variations can induce up to 75% uncertainty in catalytic CH_4 conversion rates. It is important to note that the PCE-ANN framework is fuel- and reactor-agnostic, offering a versatile computational tool applicable to a wide range of catalytic processes where UQ is critical for robust system design and operation. Future investigations could focus on exploring different catalyst materials and their influence on UQ, assessing the impact of trace impurities such as dust, NO_x, H_2O, and common poisons (e.g., H_2S, SO_2) on conversion rate uncertainty and system reliability, and developing more comprehensive models to simulate catalyst deactivation and transient operating conditions typical of VAM systems. Additionally, evaluating the framework's ability to generalise across channel geometries and validating these simulations experimentally would provide valuable insights into the practical implications of UQ in catalytic methane combustion.

5. Acknowledgements

Israfil Soyler acknowledges the Republic of Türkiye Ministry of National Education for their financial support through a PhD scholarship. N. Karimi acknowledges the financial support provided by EPSRC through grant number EP/X019551/1.

6. Declaration

During the preparation of this work the authors used ChatGPT in order to improve the clarity of text in some parts of the manuscript. After using this service, the authors reviewed and edited the content as needed and take full responsibility for the content of the publication.

References

[1] IPCC, Climate change 2007, Available online, accessed: November 18, 2025(2008).
URL https://www.ipcc.ch/site/assets/uploads/2018/05/ar4-wg1-errata.pdf

[2] International Energy Agency, World energy outlook 2024, Report, IEA, Paris, license: Report: CC BY 4.0; Annex A: CC BY NC SA 4.0 (2024).

[3] International Energy Agency, Global methane tracker 2024, Report, IEA, Paris, licence: CC BY 4.0 (2024).
URL https://www.iea.org/reports/global-methane-tracker-2024

[4] U. N. Publications, Best Practice Guidance for Effective Methane Drainage and Use in Coal Mines, ECE energy series, United Nations Economic Commission for Europe, 2016.
URL https://books.google.com.tr/books?id=HfwEDcx6K3YC

[5] Z. Yang, M. Z. Hussain, P. Marín, Q. Jia, N. Wang, S. Ordóñez, Y. Zhu, Y. Xia, Enrichment of low concentration methane: an overview of ventilation air methane, Journal of Materials Chemistry A 10 (12) (2022) 6397–6413.

[6] J. H. Lee, D. L. Trimm, Catalytic combustion of methane, Fuel processing technology 42 (2-3) (1995) 339–359.

[7] A. Setiawan, E. M. Kennedy, M. Stockenhuber, Development of combustion technology for methane emitted from coal-mine ventilation air systems, Energy Technology 5 (4) (2017) 521–538.

[8] H. N. Sharma, V. Sharma, A. B. Mhadeshwar, R. Ramprasad, Why pt survives but pd suffers from so x poisoning?, The journal of physical chemistry letters 6 (7) (2015) 1140–1148.

[9] X. Feng, L. Jiang, D. Li, S. Tian, X. Zhu, H. Wang, C. He, K. Li, Progress and key challenges in catalytic combustion of lean methane, Journal of Energy Chemistry 75 (2022) 173–215.

[10] S. Su, X. Yu, A 25ákwe low concentration methane catalytic combustion gas turbine prototype unit, Energy 79 (2015) 428–438.

[11] R. Burch, P. Loader, Investigation of pt/al2o3 and pd/al2o3 catalysts for the combustion of methane at low concentrations, Applied Catalysis B: Environmental 5 (1-2) (1994) 149–164.

[12] X. Wei, J. Kang, L. Gan, W. Wang, L. Yang, D. Wang, R. Zhong, J. Qi, Recent advances in co3o4-based composites: Synthesis and application in combustion of methane, Nanomaterials 13 (13) (2023). doi:10.3390/nano13131917.

[13] X. Xu, W. Liu, H. Liu, Y. Li, X. Gao, B. Lu, J. Qi, Z. Li, J. Han, Y. Yan, Self-supporting characteristics in hierarchical monolith catalyst with highly accessible active sites for boosting lean methane catalytic oxidation, Fuel 405 (2026) 136576. doi:https://doi.org/10.1016/j.fuel.2025.136576.

[14] L. He, Y. Fan, J. Bellettre, J. Yue, L. Luo, Catalytic methane combustion in plate-type microreactors with different channel configurations: An experimental study, Chemical Engineering Science 236 (2021) 116517.

[15] G. Hunt, N. Karimi, A. Mehdizadeh, Intensification of ultra-lean catalytic combustion of methane in microreactors by boundary layer interruptions–a computational study, Chemical Engineering Science 242 (2021) 116730.

[16] V. Dupont, F. Moallemi, A. Williams, S.-H. Zhang, Combustion of methane in catalytic honeycomb monolith burners, International journal of energy research 24 (13) (2000) 1181–1201.

[17] S. Kumaresh, M. Y. Kim, Numerical investigation of catalytic combustion in a honeycomb monolith with lean methane and air premixtures over the platinum catalyst, International Journal of Thermal Sciences 138 (2019) 304–313.

[18] O. Deutschmann, F. Behrendt, J. Warnatz, Modelling and simulation of heterogeneous oxidation of methane on a platinum foil, Catalysis Today 21 (2-3) (1994) 461–470.

[19] X. Jiang, D. Mira, D. Cluff, The combustion mitigation of methane as a non-co2 greenhouse gas, Progress in Energy and Combustion Science 66 (2018) 176–199.

[20] S. Rahimi, M. Ataee-pour, H. Madani, S. M. Aminossadati, Investigating the impact of gas emission uncertainty on airflow distribution in an auxiliary ventilation system using cfd and monte-carlo simulation, Building and Environment 204 (2021) 108165.

[21] L. He, Y. Fan, J. Bellettre, J. Yue, L. Luo, A review on catalytic methane combustion at low temperatures: Catalysts, mechanisms, reaction conditions and reactor designs, Renewable and Sustainable Energy Reviews 119 (2020) 109589.

[22] P. Thevenin, A. Ersson, H. Kušar, P. Menon, S. G. Järås, Deactivation of high temperature combustion catalysts, Applied Catalysis A: General 212 (1-2) (2001) 189–197.

[23] H. Ozcan, E. Kayabasi, Thermodynamic and economic analysis of a synthetic fuel production plant via co2 hydrogenation using waste heat from an iron-steel facility, Energy Conversion and Management 236 (2021) 114074.

[24] H. Wang, Uncertainty quantification and minimization, in: Computer Aided Chemical Engineering, Vol. 45, Elsevier, 2019, pp. 723–762.

[25] J. C. Helton, J. D. Johnson, W. L. Oberkampf, C. J. Sallaberry, Representation of analysis results involving aleatory and epistemic uncertainty, International Journal of General Systems 39 (6) (2010) 605–646.

[26] H. Wang, D. A. Sheen, Combustion kinetic model uncertainty quantification, propagation and minimization, Progress in Energy and Combustion Science 47 (2015) 1–31.

[27] T. Turányi, T. Nagy, I. G. Zsély, M. Cserháti, T. Varga, B. T. Szabó, I. Sedyo, P. T. Kiss, A. Zempleni, H. J. Curran, Determination of rate parameters based on both direct and indirect measurements, International Journal of Chemical Kinetics 44 (5) (2012) 284–302.

[28] O. M. Knio, H. N. Najm, R. G. Ghanem, et al., A stochastic projection method for fluid flow: I. basic formulation, Journal of computational Physics 173 (2) (2001) 481–511.

[29] R. Tripathy, I. Bilionis, M. Gonzalez, Gaussian processes with built-in dimensionality reduction: Applications to high-dimensional uncertainty propagation, Journal of Computational Physics 321 (2016) 191–223.

[30] C. E. Üstün, A. Paykani, Probabilistic machine learning framework for chemical source term integration with gaussian processes: H2/air auto-ignition case, International Journal of Hydrogen Energy 81 (2024) 47–55.

[31] K. Zhang, X. Jiang, An investigation of fuel variability effect on bio-syngas combustion using uncertainty quantification, Fuel 220 (2018) 283–295.

[32] H. N. Najm, Uncertainty quantification and polynomial chaos techniques in computational fluid dynamics, Annual review of fluid mechanics 41 (1) (2009) 35–52.

[33] H. N. Najm, B. J. Debusschere, Y. M. Marzouk, S. Widmer, O. Le Maître, Uncertainty quantification in chemical systems, International journal for numerical methods in engineering 80 (6-7) (2009) 789–814.

[34] M. T. Reagan, H. N. Najm, P. P. Pébay, O. M. Knio, R. G. Ghanem, Quantifying uncertainty in chemical systems modeling, International journal of chemical kinetics 37 (6) (2005) 368–382.

[35] Y. Tang, M. Hassanaly, V. Raman, B. Sforzo, J. Seitzman, A comprehensive modeling procedure for estimating statistical properties of forced ignition, Combustion and Flame 206 (2019) 158–176.

[36] I. Soyler, K. Zhang, C. Duwig, X. Jiang, N. Karimi, Uncertainty quantification of the premixed combustion characteristics of nh3/h2/n2 fuel blends, International Journal of Hydrogen Energy 48 (38) (2023) 14477–14491.

[37] I. Soyler, K. Zhang, X. Jiang, N. Karimi, Effects of compositional uncertainties in cracked nh3/biosyngas fuel blends on the combustion characteristics and performance of a combined-cycle gas turbine: A numerical thermokinetic study, International Journal of Hydrogen Energy 69 (2024) 504–517.

[38] K. Zhang, X. Jiang, Uncertainty quantification of fuel variability effects on high hydrogen content syngas combustion, Fuel 257 (2019) 116111.

[39] K. Zhang, X. Jiang, An assessment of fuel variability effect on biogas-hydrogen combustion using uncertainty quantification, International Journal of Hydrogen Energy 43 (27) (2018) 12499–12515.

[40] M. Anwar, I. Soyler, N. Karimi, Machine learning-enhanced uncertainty quantification for renewable-powered hybrid green ammonia and refrigeration systems: Techno-economic and environmental effects, Journal of Cleaner Production 527 (2025) 146702.

doi:https://doi.org/10.1016/j.jclepro.2025.146702.
URL https://www.sciencedirect.com/science/article/pii/S0959652625020529

[41] C. E. Üstün, M. R. Herfatmanesh, A. Valera-Medina, A. Paykani, Applying machine learning techniques to predict laminar burning velocity for ammonia/hydrogen/air mixtures, Energy and AI 13 (2023) 100270.

[42] C. E. Üstün, S. Eckart, A. Valera-Medina, A. Paykani, Data-driven prediction of laminar burning velocity for ternary ammonia/hydrogen/methane/air premixed flames, Fuel 368 (2024) 131581.

[43] Y. Cui, Q. Wang, H. Liu, Z. Zheng, H. Wang, Z. Yue, M. Yao, Development of the ignition delay prediction model of n-butane/hydrogen mixtures based on artificial neural network, Energy and AI 2 (2020) 100033.

[44] F. N. Alotaibi, A. S. Berrouk, M. Saeed, Optimization of yield and conversion rates in methane dry reforming using artificial neural networks and the multiobjective genetic algorithm, Industrial & Engineering Chemistry Research 62 (42) (2023) 17084–17099.

[45] L. Zhou, Y. Song, W. Ji, H. Wei, Machine learning for combustion, Energy and AI 7 (2022) 100128.

[46] B. Debusschere, K. Sargsyan, C. Safta, K. Chowdhary, The uncertainty quantification toolkit (uqtk), in: R. Ghanem, D. Higdon, H. Owhadi (Eds.), Handbook of Uncertainty Quantification, Springer, 2017, pp. 1807–1827.
URL http://www.springer.com/us/book/9783319123844

[47] D. Xiu, G. E. Karniadakis, The wiener–askey polynomial chaos for stochastic differential equations, SIAM journal on scientific computing 24 (2) (2002) 619–644.

[48] F. Xiong, S. Chen, Y. Xiong, Dynamic system uncertainty propagation using polynomial chaos, Chinese Journal of Aeronautics 27 (5) (2014) 1156–1170.

[49] S. Kucherenko, S. Song, Different numerical estimators for main effect global sensitivity indices, Reliability Engineering & System Safety 165 (2017) 222–238.

[50] O. Deutschmann, L. Maier, U. Riedel, A. Stroemman, R. Dibble, Hydrogen assisted catalytic combustion of methane on platinum, Catalysis today 59 (1-2) (2000) 141–150.

[51] D. G. Goodwin, H. K. Moffat, R. L. Speth, Cantera: An object-oriented software toolkit for chemical kinetics, thermodynamics, and transport processes (2018).

[52] I. Cornejo, P. Nikrityuk, R. E. Hayes, Heat and mass transfer inside of a monolith honeycomb: From channel to full size reactor scale, Catalysis Today 383 (2022) 110–122.

[53] P. Gélin, M. Primet, Complete oxidation of methane at low temperature over noble metal based catalysts: a review, Applied Catalysis B: Environmental 39 (1) (2002) 1–37.